

Broadband ptychographic imaging with an accurately sampled spectrumRuifan Liu ¹, Wei Cao ^{1,*}, Qijun You,¹ Yun Gao,¹ Fucai Zhang ², Qing Liao,³ and Peixiang Lu^{1,4}¹*School of Physics and Wuhan National Laboratory for Optoelectronics, Huazhong University of Science and Technology, Wuhan 430074, China*²*Department of Electrical and Electronic Engineering, Southern University of Science and Technology, Shenzhen 518055, China*³*Hubei Key Laboratory of Optical Information and Pattern Recognition, Wuhan Institute of Technology, Wuhan 430205, China*⁴*Optics Valley Laboratory, Wuhan 430074, China*

(Received 1 December 2022; revised 6 March 2023; accepted 10 March 2023; published 20 March 2023)

Ptychography, a lensless imaging technology with large field of view (FOV), has been extensively developed in the past decades. However, the demanding coherence of the light source restrains its application in the field of ultrafast imaging, as short light pulses have broad spectral bandwidth and thus poor temporal coherence. Here, we demonstrated the implementation of ultrafast imaging with large FOV by monochromatizing the polychromatic ptychographic diffraction patterns. This scheme relaxes the requirement of bandwidth and successfully realizes the millimeter-scale FOV imaging using ultrashort pulses, while maintaining the good spatial resolution of the order of diffraction limit. Due to the use of a precisely sampled spectrum, the illumination information can be accurately captured allowing more reliable imaging process. Experimental results show that satisfactory spatial resolution can still be achieved even for a relative bandwidth up to 20%. Our work demonstrates the potential of ultrafast diffraction imaging with a large FOV.

DOI: [10.1103/PhysRevA.107.033510](https://doi.org/10.1103/PhysRevA.107.033510)**I. INTRODUCTION**

As a scanning coherent diffraction imaging (CDI) scheme with a large FOV, ptychography can reconstruct the information of an object and probe simultaneously and has more easily determined prior conditions [1–5]. Nowadays, it is widely used in high-precision structure measurement [6,7], surface topography detection [8,9], and beam diagnosis [10,11]. Because of its lensless structure, it can be perfectly applied to extreme ultraviolet (XUV) and even the x-ray region [12–14]. However, like most optical microscopy imaging schemes, the narrow bandwidth is a necessary presupposition for CDI [15]. Once the bandwidth becomes broad, the effect of different wavelengths is that the pattern becomes blurred and a lot of effective information is lost [16–19]. The high dependence on bandwidth limits the applicability of this unique imaging technique to ultrafast imaging [20–22].

Recently, several groups implemented CDI using polychromatic light sources [23–25]. Abbey *et al.* proposed a polychromatic phase retrieval algorithm to successfully reconstruct nanoscale samples with high resolution using a broadband source. This approach, dubbed “polyCDI,” requires *a priori* knowledge of the power spectrum of the illumination and the initial support and the theoretical upper limit of the bandwidth can be 11% [23]. However, as a single frame imaging scheme, the FOV achieved by polyCDI is rather limited. Therefore, ptychographic imaging has been an possible solution to fulfill large FOV incorporating polychromatic light source. Batey *et al.* proposed the pty-

chographical information multiplexing (PIM) in which the contributions from multiple probes with different wavelengths can be separable within the ptychographic data set, this allows one to recover the spectral response of an object with both spatial and spectral resolution [26]. Very recently, Rana *et al.* reported an improved version of the broadband ptychographic algorithm SPIRE that allowed the simultaneous reconstruction of the spectrum, probes, and objects at different wavelengths [24]. In this work, only 17 probe modes with different frequencies were reconstructed experimentally. Increasing the number of modes not only requires heavier computation but also may lead to theoretically unsolvable phase retrieval problems [27–30]. Therefore, in both polyCDI and SPIRE, the spectrum of the broadband light source usually requires being sparsely sampled and the missing frequency components may cause error during the phase retrieval process, which greatly limits its application in spectrum sensitive measurements.

The previous methods generated a polychromatic diffraction pattern from the monochromatic diffraction pattern. The reconstruction will be successful if the iterative phase retrieval converges while satisfying the intensity constrain. Recently, Huijts *et al.* proposed the broadbandCDI, in which they reproduced the monochromatic diffraction pattern from the detected polychromatic diffraction pattern [25]. The monochromatic pattern can be obtained by conjugate gradient least squares (CGLS) [31], which is suitable for any CDI schemes and achieves almost the same resolution at 11% bandwidth as the monochromatic source.

Here, we introduce monochromatization of the polychromatic diffraction pattern into ptychography to achieve an ultrafast imaging with a large FOV. It incorporates the merits of high toleration to the broad bandwidth of CGLS and

*weicao@hust.edu.cn

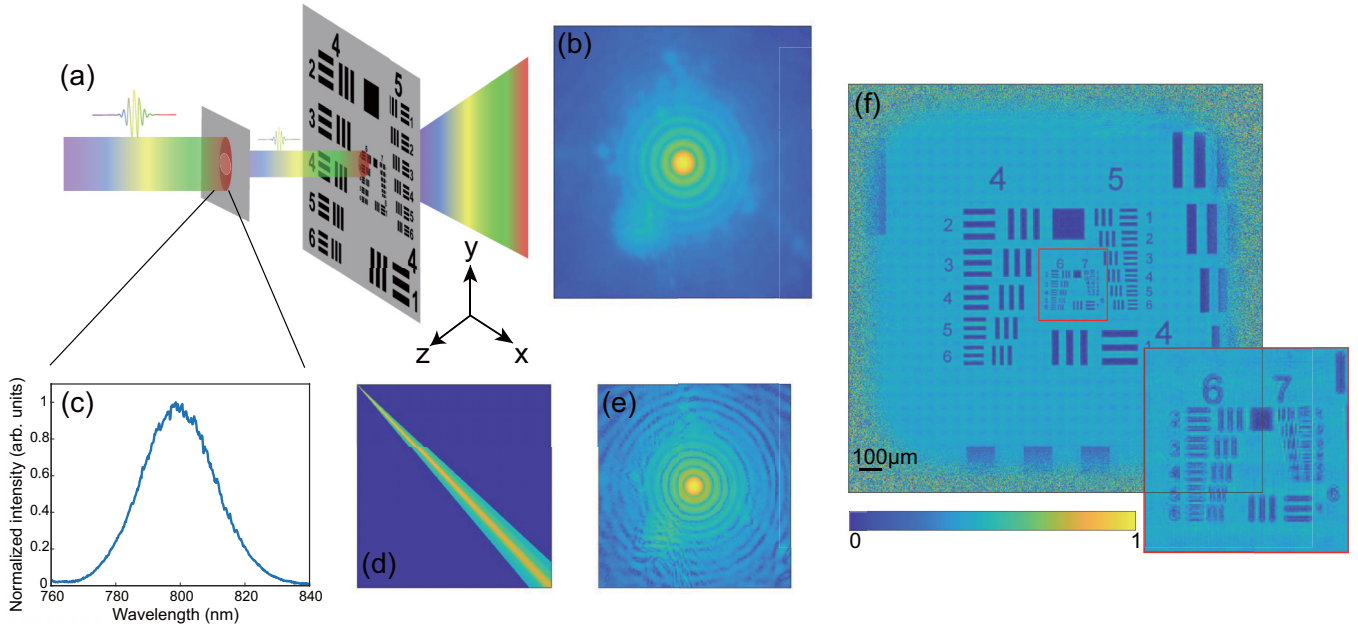


FIG. 1. Experimental method and the flowchart of mono-PIE. (a) Schematic diagram of the experimental setup. The pulses propagate through a precision pinhole and illuminate the object installed on a two-dimensional electronic positioning stage and the CMOS detects the diffraction pattern generated at each scanning position. (b) Detected diffraction patterns. (c) Spectrum of the pulses used in the experiment. (d) Constructed diffraction matrix. As a schematic diagram, only the data with an x and y pixel value of 1 is shown and the actual diffraction matrix should consider the contribution of all pixels. (e) Monochromatic patterns obtained by CGLS. (f) The amplitude of the object obtained after reconstruction of (e) by ePIE. The inset is the enlarged image of the central portion.

the high robustness to the noise of ptychography [25,32,33]. With an accurately sampled spectrum, the method effectively avoids the loss of frequency component, such as the fine peaks that may exist in the supercontinuum spectrum, and exhibits extremely high tolerance to a broad bandwidth. The results show that, even with a bandwidth close to 20%, it can still achieve good spatial resolution with large FOV. The ultrashort pulses were used in our experiment, so this method can be effectively applied to explore the spatiotemporal information of ultrafast dynamic processes by the pump-probe technique [34].

II. PRINCIPLE AND METHOD

Considering a broadband pulsed light diffracted by an object, if no significant absorption occurs in the spectral range, the diffraction patterns in far field at different frequencies are related mostly by a scaling factor determined by the ratio of the respective wavelengths. Moreover, the exposure time of the image sensor is usually much longer than the pulse period, so the final detected pattern will be equivalent to an incoherent superposition of the diffraction patterns of all wavelengths [18,35]

$$P(k_x, k_y) = \sum_{\lambda} \frac{I(\lambda)}{\lambda^2 z^2} |\varphi_{\lambda}(k_x, k_y)|^2 + N(\lambda, k_x, k_y). \quad (1)$$

The detected polychromatic diffraction pattern P at the detector distance z comes from diffraction φ_{λ} of different wavelengths λ and experimental noise N since the φ_{λ} is just the scaling of the identical distribution at spatial frequencies k_x and k_y [36]. The incoherent summation in Eq. (1) can

be expressed by the product between the monochromatized diffraction pattern and a spectrum-dependent matrix D , as shown in Ref. [25], and the detected diffraction can be written as

$$P(k_x, k_y) = D_{ijuv}(I, d)M_{uv}(k_x, k_y) + N(\lambda, k_x, k_y). \quad (2)$$

The diffraction matrix D is a four-dimensional tensor with i , j , u , and v as subscripts, and its construction is only related to the power spectrum I and the number of pixels d from the diffraction center to the edge of the monochromatic diffraction pattern M at the central wavelength. Using CGLS to solve Eq. (2), the monochromatic diffraction pattern M can be obtained. However, due to the existence of noise N , the iteration number of CGLS must be reasonably selected, otherwise it will tend to diverge due to the dominance of noise [37]. In addition, due to its semi-convergence character, the obtained monochromatic diffraction pattern M inevitably has some error from the ideal value, which is a very tricky problem for conventional noise-sensitive CDI schemes. Therefore, we apply this method to ptychography, which has excellent noise tolerance and large FOV. Each detected diffraction pattern is monochromatized and then used as input in ptychographic iterative algorithm. We refer to this method as monochromatized PIE (mono-PIE).

The flowchart is shown in Fig. 1, and its experimental setup [Fig. 1(a)] is completely consistent with conventional ptychography [3,38], except that the incident light source is no longer limited by the narrow bandwidth and ultrashort pulses are adopted. The incident light passes through a small pinhole and illuminates the object moved in the X - Y plane with a two-dimensional (2-D) motorized stage with high precision.

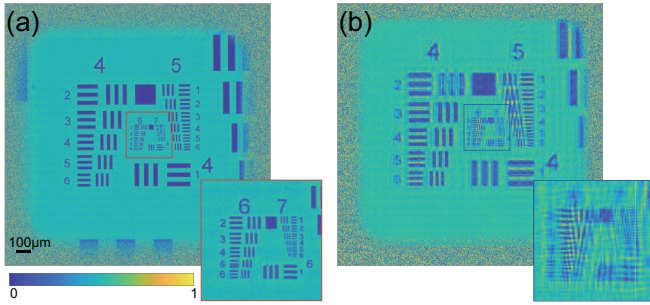


FIG. 2. Comparison of the reconstructed objects illuminated with the (a) 532-nm CW laser and (b) the pulsed laser with 3.75% bandwidth. The insets are the enlarged images of the central portion.

An image sensor is placed downstream from the object to detect diffraction patterns at different positions. Mono-PIE first detects diffraction patterns and the spectrum [Figs. 1(b) and 1(c)], the spectrum is only utilized once to construct the diffraction matrix D [Fig. 1(d)], and thus can be sampled as finely as desired. Multiple images are detected at the same position with different exposure times to obtain high dynamic range (HDR) patterns [39]. With the constructed diffraction matrix D and detected diffraction patterns P known, the monochromatized diffraction patterns M [Fig. 1(e)] can be calculated using the CGLS method. All the monochromatized diffraction images at different positions are used as input for ePIE or any suitable ptychography iterative algorithm, and the reconstructed result with greatly improved resolution will be obtained [Fig. 1(f)].

III. RESULTS AND DISCUSSION

To demonstrate the significant impact of the bandwidth on the result of CDI, we used a 532-nm monochromatic light and ultrashort pulses (Coherent Vitar-T) with bandwidth $\Delta\lambda/\lambda = 3.75\%$ [Fig. 1(c)] to carry out experiments on a USAF1951 resolution test chart, respectively. The ePIE algorithm is directly applied to the detected diffraction patterns for reconstruction. In addition the diameter of the precision pinhole is $200\mu\text{m}$ and the step size of the movement is $57.6\mu\text{m}$. We use a complementary metal-oxide semiconductor (CMOS) (2048×2048 pixels, $11 \times 11\mu\text{m}$) placed 8.3-cm downstream from the object to detect a total of 21×21 positions to achieve a large FOV of 1.35×1.35 mm. Therefore, the numerical aperture (NA) is 0.135, corresponding to an Abbe limit of about 3.7 wavelengths [40].

It can be seen that the 532-nm light achieves a good reconstructed result [Fig. 2(a)], while the result of the ultrashort pulses is significantly worse [Fig. 2(b)]. This is simply because the intensity constraint, which is so critical for ptychography to be successful, no longer applies in the case of a broadband light source. In essence, the goal of phase retrieval is to search for a local optimal solution by iterating alternately in real and reciprocal space based on some prior information [41,42]. For ptychography under a broadband light source, real space takes the high redundancy of information at adjacent positions as the constraint, which is consistent with the monochromatic case. However, for the diffraction plane, the change of constraint makes the convergence of the iteration

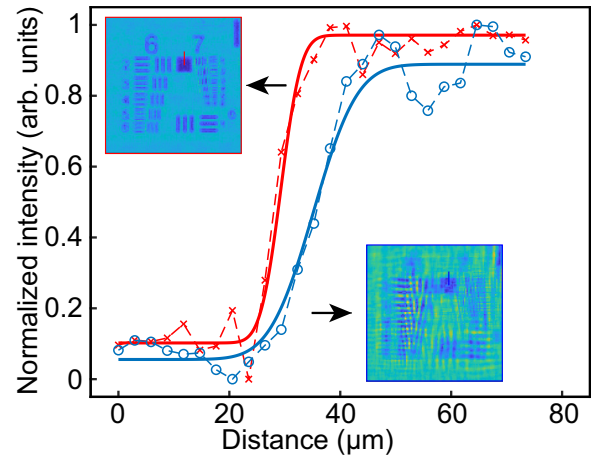


FIG. 3. Comparison of the resolution between ePIE (circle) and mono-PIE (cross) at 3.75% bandwidth. Data points are selected from the lines in the insets and fitted with error functions.

much more difficult. Even in the case of continuous wave (CW) light source, trivial ambiguity is always the main reason for the nonunique solution and makes the result of the iteration worse [43]. In addition, the traditional Fraunhofer diffraction formula, which is generally applied for phase estimation in the Fourier domain, is incompatible with broadband sources. Therefore, this is a rough reciprocal space constraint that results in a substantial reduction in spatial resolution under a broadband light source. In other words, the mismatch between phase and amplitude causes the iteration to fail to converge efficiently.

To demonstrate the effect of monochromatization on improving spatial resolution, we input the detected diffraction patterns [Fig. 1(b)] and the spectral information [Fig. 1(c)] into mono-PIE. The diffraction matrix [Fig. 1(d)] is applied to the polychromatic patterns at all positions and the monochromatic diffraction patterns [Fig. 1(e)] can be obtained with the help of the CGLS algorithm. It is evident that the initial diffraction pattern [Fig. 1(b)] from a broadband source gets blurred away from the image center and therefore loses high-frequency information in the reciprocal space. However, after the treatment with CGLS, more diffraction details are recovered in the monochromatized diffraction pattern [Fig. 1(e)]. We use the ePIE algorithm for 200 iterations and the result [Fig. 1(f)] is significantly improved compared with the one without monochromatization [Fig. 2(b)]. In the case of a broadband illuminating light source, a large amount of high spatial frequency information is lost, which causes the reconstruction of small structure details to fail, as is shown in the inset of Fig. 2(b). However, mono-PIE uses monochromatization to recover the lost high spatial frequency information and then the final result [Fig. 1(f)] is almost the same as the one using a monochromatic laser source [Fig. 2(a)], but yields a very high temporal resolution. This proves the validity of mono-PIE on improving spatial resolution as expected.

We quantitatively analyze the effect of mono-PIE on resolution improvement. The line cuts around specific regions (labeled with a red or blue line in the insets of Fig. 3) of the reconstructed object are fitted with error functions to

evaluate the resolution and the results are shown in Fig. 3. With the bandwidth $\Delta\lambda/\lambda = 3.75\%$, mono-PIE improved the resolution of ptychography from $14.68\ \mu\text{m}$ to $6.75\ \mu\text{m}$, which achieves a resolution improvement of nearly 120%.

For mono-PIE, the monochromatized result M is equivalent to obtaining a smaller bandwidth pattern at the cost of introducing some errors. Due to the excellent robustness of ptychography, the highly redundant information of the adjacent position enables it to effectively reconstruct the object even in the case of high noise [44]. Therefore, mono-PIE can achieve better convergence with a faster speed because its reciprocal space constraint is more precise than those discussed in the previous section. This combination of the advantages of monochromatization and ptychography not only realizes millimeter-scale FOV, but also has better tolerance of bandwidth as we will see below. Since most ultrafast light sources now produce stable pulses, we can use the same diffraction matrix no matter how many experiments are carried out. Therefore, the diffraction matrix only needs to be constructed once at the beginning, which will greatly reduce the time required by mono-PIE. It should be noted that the overlap ratio used in our measurement is 71.2%, which is also an advantage over previously reported studies that typically required an overlap ratio over 90% to achieve reliable phase retrieval [18,24,26].

Importantly, mono-PIE is able to reconstruct the probe as well, as is shown in the Appendix. Also our results show that mono-PIE reconstructs the probe even better than the object. Because, in a complete ePIE iteration, the number of reconstructions of the probe is much larger than the object, therefore, mono-PIE has an excellent application prospect for pulse diagnosis in a broadband light source.

Furthermore, we verify the tolerance of mono-PIE to bandwidth. We repeat the above experiments using ultrashort pulses with different bandwidths $\Delta\lambda/\lambda = 7.51\%$, 12.66%, and 15.82% [Fig. 4(a), blue, orange, and yellow lines], respectively. While the bandwidth continues to increase, resolution decreases as expected [Figs. 4(b)–4(d)]. We are surprised to find that mono-PIE was extremely robust against variation of the bandwidth. Even at a bandwidth of 15.82%, the reconstructed result [Fig. 4(d)] is still better than the case without monochromatization at a bandwidth of 3.75% [Fig. 2(b)].

In principle, mono-PIE sets no limit on the number of sampling points in the spectrum and more precise sampling will make the diffraction closer to the continuous sampling under real conditions. In our experiment, the spectrum contains 1096 wavelengths ranging from 700 to 900 nm with a sampling interval of about 0.18 nm, which is an advantage that cannot be satisfied by reported schemes such as polyCDI and SPIRE, which only sampled tens of wavelengths in their experiments. The accurately sampled spectrum is a powerful constraint, resulting in a significant reduction in the number of unknown quantities in phase retrieval. Moreover, the more accurately sampled the spectrum, the more effective this constraint will be because it contains more valid prior information. In addition, this feature makes the number of modes have little impact on mono-PIE. The error of intensity constrain caused by the limited modes will be greatly reduced because of the accurately sampled spectrum. This also allows mono-PIE to be used even in a complicated spectrum, such as when the

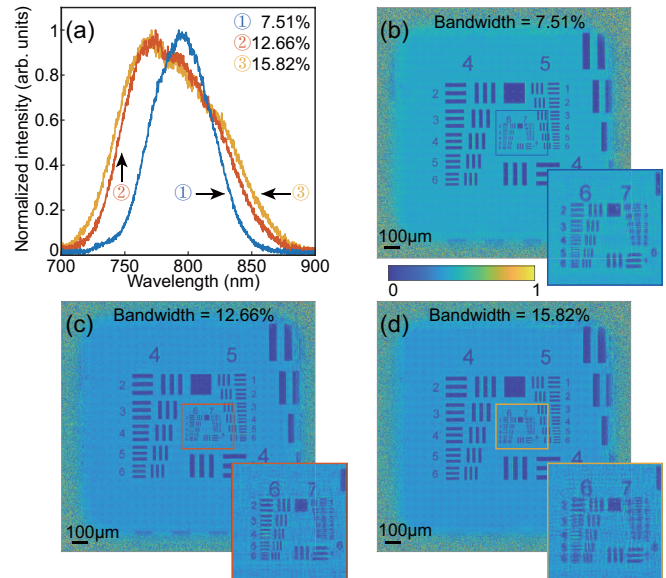


FIG. 4. Experimental results using mono-PIE under different bandwidths. (a) The spectra of used ultrashort pulses. The bandwidth $\Delta\lambda/\lambda$ of the blue, orange, and yellow lines labeled 1, 2, and 3 are 7.51%, 12.66%, and 15.82%, respectively. (b)–(d) The amplitude of object reconstructed by mono-PIE under 7.51%, 12.86%, and 15.82% bandwidth, respectively. The insets are the enlarged images of the central portion.

spectrum has sharp spikes and dips. However, most broadband CDI algorithms may not be available in this condition as they can face theoretically unsolvable phase retrieval problems with the increasing number of modes. However, the tolerance of bandwidth for mono-PIE is not unlimited. Practical issues still need to be considered while using the current method.

First, as the spectrum gets broader, it magnifies some subtle experimental errors. Mono-PIE only needs to detect spectrum and diffraction patterns. The first converts photons at different wavelengths into electrons through a linear CCD, and the response of the second to different wavelengths is affected by quantum efficiency. Therefore, both of them introduce more errors into the data as the frequency component of the spectrum increases, and ultimately reduce the resolution of the reconstruction. Second, the broader the spectrum, the more likely there is partial absorption in the sample [45,46]. Once partial absorption occurs, the constructed diffraction matrix D will no longer accurately depict the relationship between the monochromatic and polychromatic diffractions. If D is no longer correct for the description of the diffraction relation, this will introduce a large amount of initial error. Thus this error will be further brought to the calculation in CGLS, so the iteration will be difficult to obtain satisfactorily.

The last reason comes from the mono-PIE itself. Although the wavelength of the monochromatized pattern M can be arbitrarily chosen before the reconstruction of the diffraction matrix, we still choose the central wavelength as the output. However, for the patterns corresponding to a shorter wavelength, the outermost high spatial frequency information cannot be obtained by scaling, so the data can only be padded with zeros [25]. Therefore, for the frequency components whose wavelengths are shorter than the central wavelength,

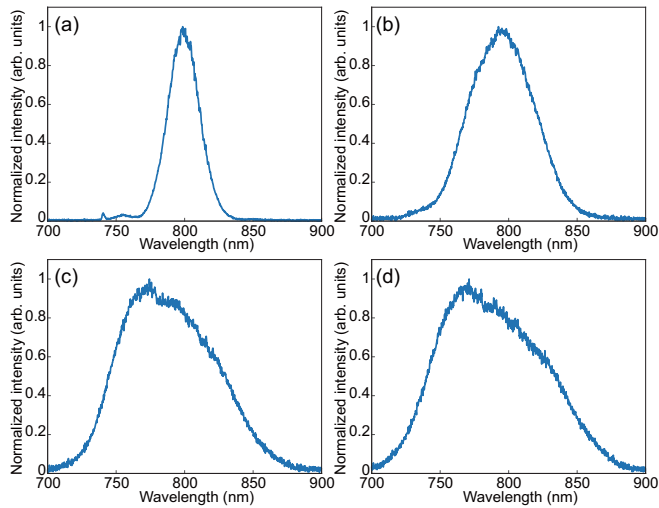


FIG. 5. The spectra of used ultrashort pulses. (a)–(d) The bandwidth $\Delta\lambda/\lambda = 3.75\%$, 7.51% , 12.66% , and 15.82% .

the information of the high spatial frequencies is inevitably lost. As the bandwidth becomes broader, this loss gradually intensifies and eventually significantly affects the quality of the data. Although choosing the shortest wavelength as the output of monochromatic pattern M can avoid this problem, it will introduce a great error. Because the intensity of the power spectrum at the edge is close to the background noise, using this as a reference and scaling to obtain the diffraction pattern will also amplify the noise. So it is a tradeoff between

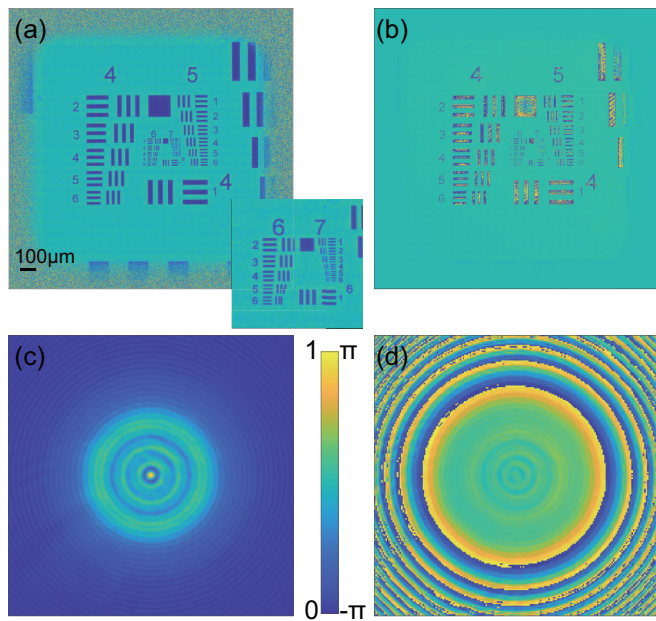


FIG. 6. Reconstructed results of 532-nm CW laser. (a) The amplitude of the reconstructed object. The inset is the enlarged image of the central portion. (b) The phase of the reconstructed object. (c) The amplitude of the reconstructed probe. (d) The phase of the reconstructed probe.

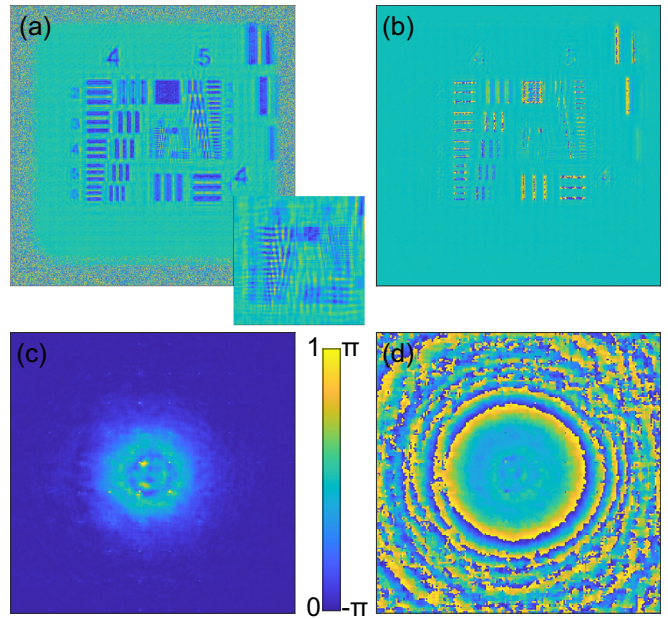


FIG. 7. Same as Fig. 6, but for ePIE at 3.75% bandwidth.

wavelength and light intensity. The combined effect of these reasons is that the resolution becomes degraded.

IV. CONCLUSION

In conclusion, we demonstrated a millimeter-scale broadband diffractive imaging method, mono-PIE. Compared with traditional ptychography, this method only needs to additionally detect spectral information without other, tedious steps. We make use of the monochromatic result of CGLS and the high robustness of ptychography. Since the number of wavelengths included in the spectrum has little effect on the use of

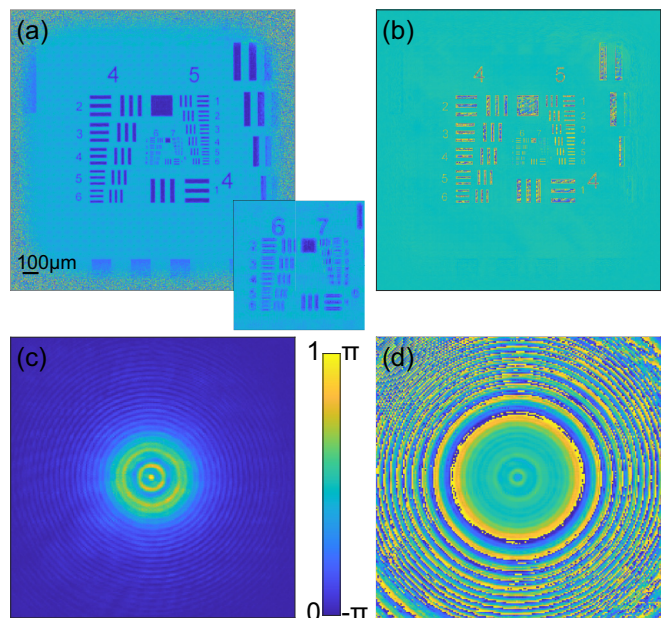


FIG. 8. Same as Fig. 6, but for mono-PIE at 3.75% bandwidth.

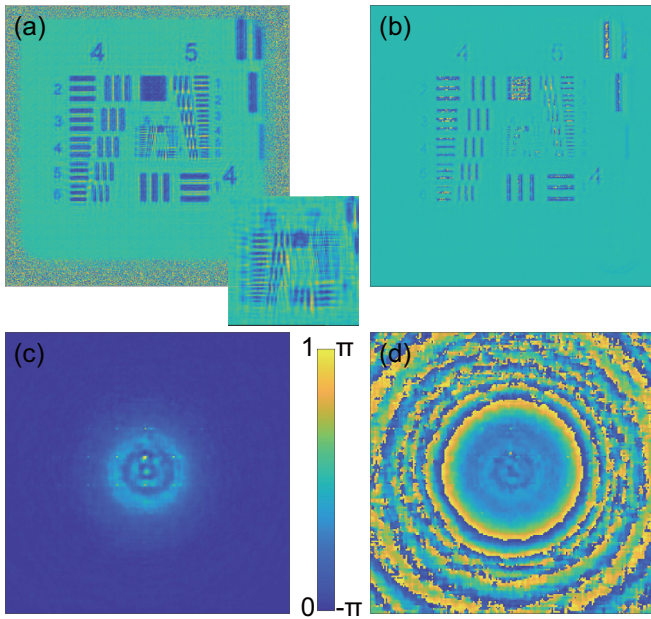


FIG. 9. Same as Fig. 6, but for ePIE at 7.51% bandwidth.

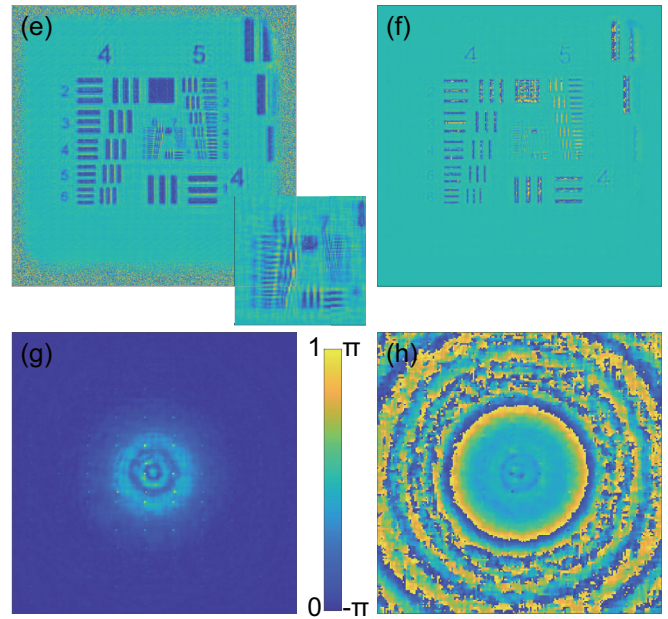


FIG. 11. Same as Fig. 6, but for ePIE at 12.66% bandwidth.

mono-PIE, the accurately sampled spectrum can be adopted as a major advantage to recover the object from the polychromatic diffraction patterns. Even when the bandwidth is close to 20%, a significant resolution improvement is still achieved. Moreover, compared with the results of broadbandCDI based on single frame diffraction, the field of view is enlarged by more than 50 times. As a proof-of-principle experiment, we used femtosecond laser pulses centered around 800 nm to image the target. It is believed that mono-PIE can easily achieve nanoscale spatial resolution at femtosecond or even attosecond time resolution by using ultrashort pulses with a shorter central wavelength and a larger NA. Combined with

the table-top ultrafast coherent light sources, mono-PIE can be very convenient in various applications of ultrafast science [47–49] so as to achieve the high spatial and temporal resolution simultaneously.

ACKNOWLEDGMENT

This research was supported by the National Natural Science Foundation of China under Grants No. 12274158, No. 12021004, No. 12074167, and No. 11775105, Open Foundation of Hubei Key Laboratory of Optical Informa-

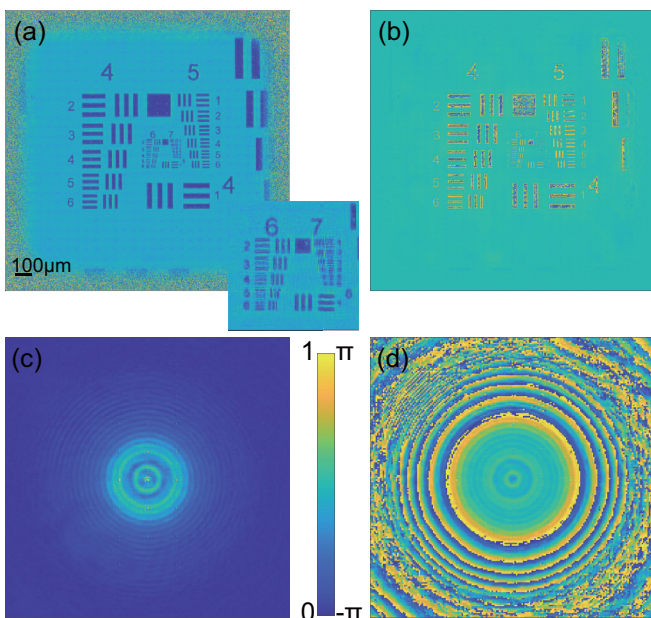


FIG. 10. Same as Fig. 6, but for mono-PIE at 7.51% bandwidth.

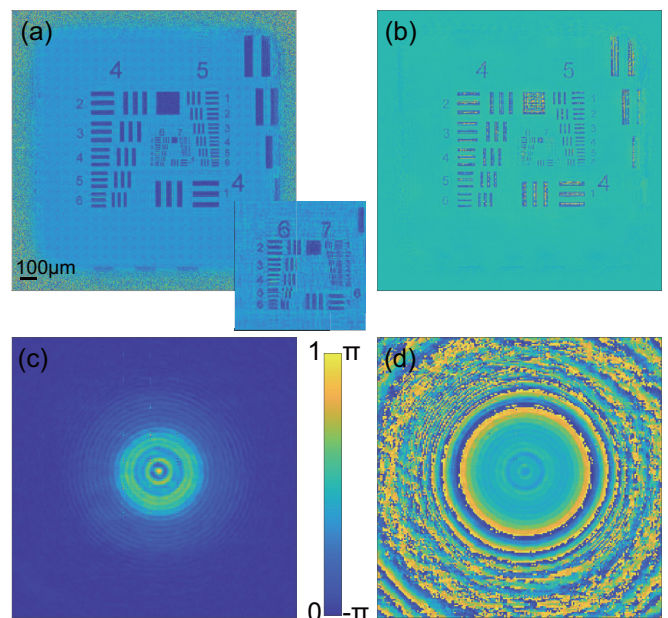


FIG. 12. Same as Fig. 6, but for mono-PIE at 12.66% bandwidth.

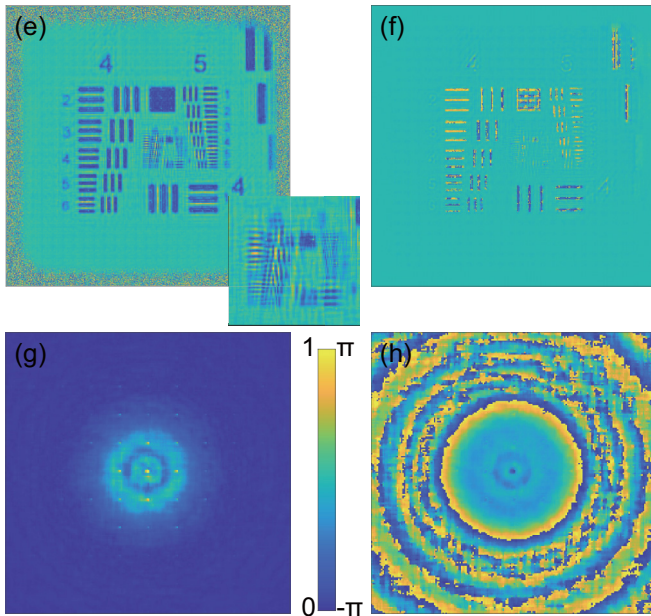


FIG. 13. Same as Fig. 6, but for ePIE at 15.82% bandwidth.

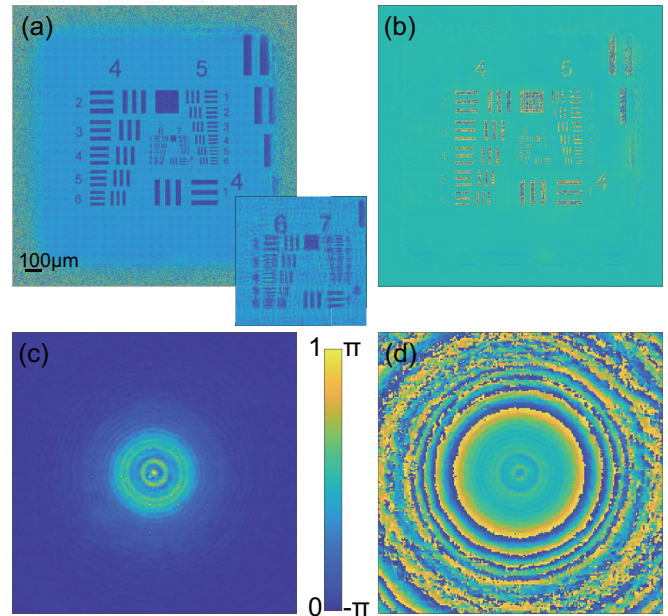


FIG. 14. Same as Fig. 6, but for mono-PIE at 15.82% bandwidth.

tion and Pattern Recognition (202101) of Wuhan Institute of Technology.

APPENDIX A: SPECTRAL INFORMATION

Figure 5 shows the spectral information used in our experiment. The sampling range is from 346 to 1033 nm (Ocean Insight, FLAME-T-VIS-NIR), but we only select the region from 700 to 900 nm. The sampling intervals fluctuate from 0.17 to 0.20 nm, with an average value of 0.1828 nm.

APPENDIX B: COMPARISON OF MONO-PIE AND EPIE

Figure 6 complements the phase and probe results of the reconstruction by ePIE at 532-nm CW laser. Figures 7 to 14 show the comparisons of the reconstruction results of mono-PIE and ePIE for the same diffraction patterns at different bandwidths, as shown in Fig. 5. Mono-PIE maintains the advantage of ptychography for the phase and probe reconstruction. Surprisingly, apart from the effect of mono-PIE on the amplitude mentioned in the main text, it is even better for the probe reconstruction. Even at 15.82% bandwidth, mono-PIE still retains the diffraction features and high spatial frequency details in the probe.

-
- [1] J. Rodenburg and H. Faulkner, A phase retrieval algorithm for shifting illumination, *Appl. Phys. Lett.* **85**, 4795 (2004).
- [2] H. M. L. Faulkner and J. M. Rodenburg, Movable Aperture Lensless Transmission Microscopy: A Novel Phase Retrieval Algorithm, *Phys. Rev. Lett.* **93**, 023903 (2004).
- [3] O. Bunk, M. Dierolf, S. Kynde, I. Johnson, O. Marti, and F. Pfeiffer, Influence of the overlap parameter on the convergence of the ptychographical iterative engine, *Ultramicroscopy* **108**, 481 (2008).
- [4] A. M. Maiden and J. M. Rodenburg, An improved ptychographical phase retrieval algorithm for diffractive imaging, *Ultramicroscopy* **109**, 1256 (2009).
- [5] P. Thibault, M. Dierolf, O. Bunk, A. Menzel, and F. Pfeiffer, Probe retrieval in ptychographic coherent diffractive imaging, *Ultramicroscopy* **109**, 338 (2009).
- [6] P. Thibault, M. Dierolf, A. Menzel, O. Bunk, C. David, and F. Pfeiffer, High-resolution scanning x-ray diffraction microscopy, *Science* **321**, 379 (2008).
- [7] D. F. Gardner, M. Tanksalvala, E. R. Shanblatt, X. Zhang, B. R. Galloway, C. L. Porter, R. Karl Jr, C. Bevis, D. E. Adams, H. C. Kapteyn, M. M. Murnane, and G. F. Mancini, Subwavelength coherent imaging of periodic samples using a 13.5 nm tabletop coherent light source, *Nat. Photonics* **11**, 259 (2017).
- [8] D. Claus, D. J. Robinson, D. G. Chetwynd, Y. Shuo, W. T. Pike, J. J. D. J. T. Garcia, and J. M. Rodenburg, Dual wavelength optical metrology using ptychography, *J. Opt.* **15**, 035702 (2013).
- [9] B. Zhang, D. F. Gardner, M. D. Seaberg, E. R. Shanblatt, H. C. Kapteyn, M. M. Murnane, and D. E. Adams, High contrast 3d imaging of surfaces near the wavelength limit using tabletop euv ptychography, *Ultramicroscopy* **158**, 98 (2015).
- [10] M. Humphry, B. Kraus, A. Hurst, A. Maiden, and J. Rodenburg, Ptychographic electron microscopy using high-angle dark-field scattering for sub-nanometre resolution imaging, *Nat. Commun.* **3**, 730 (2012).
- [11] F. Seiboth, A. Schropp, M. Scholz, F. Wittwer, C. Rödel, M. Wünsche, T. Ullsperger, S. Nolte, J. Rahomäki, K. Parfeniukas, S. Giakoumidis, U. Vogt, U. Wagner, C. Rau, U. Boesenberg, J. Garrevoet, G. Falkenberg, E. Galtier, H. Lee, and C. Schroer, Perfect x-ray focusing via fitting corrective glasses to aberrated optics, *Nat. Commun.* **8**, 14623 (2017).

- [12] M. D. Seaberg, B. Zhang, D. F. Gardner, E. R. Shanblatt, M. M. Murnane, H. C. Kapteyn, and D. E. Adams, Tabletop nanometer extreme ultraviolet imaging in an extended reflection mode using coherent fresnel ptychography, *Optica* **1**, 39 (2014).
- [13] J. M. Rodenburg, A. C. Hurst, A. G. Cullis, B. R. Dobson, F. Pfeiffer, O. Bunk, C. David, K. Jefimovs, and I. Johnson, Hard-X-Ray Lensless Imaging of Extended Objects, *Phys. Rev. Lett.* **98**, 034801 (2007).
- [14] M. Dierolf, A. Menzel, P. Thibault, P. Schneider, C. M. Kewish, R. Wepf, O. Bunk, and F. Pfeiffer, Ptychographic x-ray computed tomography at the nanoscale, *Nature (London)* **467**, 436 (2010).
- [15] J. Spence, U. Weierstall, and M. Howells, Coherence and sampling requirements for diffractive imaging, *Ultramicroscopy* **101**, 149 (2004).
- [16] I. A. Vartanyants and I. K. Robinson, Partial coherence effects on the imaging of small crystals using coherent x-ray diffraction, *J. Phys.: Condens. Matter* **13**, 10593 (2001).
- [17] G. J. Williams, H. M. Quiney, A. G. Peele, and K. A. Nugent, Coherent diffractive imaging and partial coherence, *Phys. Rev. B* **75**, 104102 (2007).
- [18] P. Thibault and A. Menzel, Reconstructing state mixtures from diffraction measurements, *Nature (London)* **494**, 68 (2013).
- [19] B. Chen, B. Abbey, R. Dilanian, E. Balaur, G. van Riessen, M. Junker, C. Q. Tran, M. W. M. Jones, A. G. Peele, I. McNulty, D. J. Vine, C. T. Putkunz, H. M. Quiney, and K. A. Nugent, Diffraction imaging: The limits of partial coherence, *Phys. Rev. B* **86**, 235401 (2012).
- [20] I. A. Vartanyants, A. Singer, A. P. Mancuso, O. M. Yefanov, A. Sakdinawat, Y. Liu, E. Bang, G. J. Williams, G. Cadenazzi, B. Abbey, H. Sinn, D. Attwood, K. A. Nugent, E. Weckert, T. Wang, D. Zhu, B. Wu, C. Graves, A. Scherz, J. J. Turner *et al.*, Coherence Properties of Individual Femtosecond Pulses of an X-Ray Free-Electron Laser, *Phys. Rev. Lett.* **107**, 144801 (2011).
- [21] L. W. Whitehead, G. J. Williams, H. M. Quiney, D. J. Vine, R. A. Dilanian, S. Flewett, K. A. Nugent, A. G. Peele, E. Balaur, and I. McNulty, Diffractive Imaging Using Partially Coherent X Rays, *Phys. Rev. Lett.* **103**, 243902 (2009).
- [22] B. Chen, R. A. Dilanian, S. Teichmann, B. Abbey, A. G. Peele, G. J. Williams, P. Hannaford, L. Van Dao, H. M. Quiney, and K. A. Nugent, Multiple wavelength diffractive imaging, *Phys. Rev. A* **79**, 023809 (2009).
- [23] B. Abbey, L. Whitehead, H. Quiney, D. Vine, G. Cadenazzi, C. Manderson, K. Nugent, E. Balaur, C. Putkunz, A. Peele, G. Williams, and I. McNulty, Lensless imaging using broadband x-ray sources, *Nat. Photonics* **5**, 420 (2011).
- [24] A. Rana, J. Zhang, M. Pham, A. Yuan, Y. H. Lo, H. Jiang, S. J. Osher, and J. Miao, Potential of Attosecond Coherent Diffractive Imaging, *Phys. Rev. Lett.* **125**, 086101 (2020).
- [25] J. Huijts, S. Fernandez, D. Gauthier, M. Kholodtsova, A. Maghraoui, K. Medjoubi, A. Somogyi, W. Boutu, and H. Merdji, Broadband coherent diffractive imaging, *Nat. Photonics* **14**, 618 (2020).
- [26] D. J. Batey, D. Claus, and J. M. Rodenburg, Information multiplexing in ptychography, *Ultramicroscopy* **138**, 13 (2014).
- [27] Y. Bruck and L. Sodin, On the ambiguity of the image reconstruction problem, *Opt. Commun.* **30**, 304 (1979).
- [28] M. Hayes, The reconstruction of a multidimensional sequence from the phase or magnitude of its fourier transform, *IEEE Transactions Acoustics, Speech, Signal Processing* **30**, 140 (1982).
- [29] R. Bates, Uniqueness of solutions to two-dimensional fourier phase problems for localized and positive images, *Computer Vision, Graphics, Image Processing* **25**, 205 (1984).
- [30] J. Miao, D. Sayre, and H. N. Chapman, Phase retrieval from the magnitude of the fourier transforms of nonperiodic objects, *J. Opt. Soc. Am. A* **15**, 1662 (1998).
- [31] P. C. Hansen, Regularization tools: A matlab package for analysis and solution of discrete ill-posed problems, *Numerical Algorithms* **6**, 1 (1994).
- [32] A. V. Martin, F. Wang, N. D. Loh, T. Ekeberg, F. R. N. C. Maia, M. Hantke, G. van der Schot, C. Y. Hampton, R. G. Sierra, A. Aquila, S. Bajt, M. Barthelmess, C. Bostedt, J. D. Bozek, N. Coppola, S. W. Epp, B. Erk, H. Fleckenstein, L. Foucar, M. Frank *et al.*, Noise-robust coherent diffractive imaging with a single diffraction pattern, *Opt. Express* **20**, 16650 (2012).
- [33] P. Godard, M. Allain, V. Chamard, and J. Rodenburg, Noise models for low counting rate coherent diffraction imaging, *Opt. Express* **20**, 25914 (2012).
- [34] A. Zewail, Femtochemistry: Atomic-scale dynamics of the chemical bond, *J. Phys. Chem. A* **104**, 5660 (2000).
- [35] H. Quiney, Coherent diffractive imaging using short wavelength light sources, *J. Mod. Opt.* **57**, 1109 (2010).
- [36] E. Wolf, New theory of partial coherence in the space-frequency domain. Part I: Spectra and cross spectra of steady-state sources, *J. Opt. Soc. Am.* **72**, 343 (1982).
- [37] J. Huang, T.-Z. Huang, X.-L. Zhao, Z.-B. Xu, and X.-G. Lv, Two soft-thresholding based iterative algorithms for image deblurring, *Inf. Sci.* **271**, 179 (2014).
- [38] F. Pfeiffer, X-ray ptychography, *Nat. Photonics* **12**, 9 (2018).
- [39] J. Steinbrener, J. Nelson, X. Huang, S. Marchesini, D. Shapiro, J. J. Turner, and C. Jacobsen, Data preparation and evaluation techniques for x-ray diffraction microscopy, *Opt. Express* **18**, 18598 (2010).
- [40] A. J. Walton, The abbe theory of imaging: An alternative derivation of the resolution limit, *Eur. J. Phys.* **7**, 62 (1986).
- [41] V. Elser, Phase retrieval by iterated projections, *J. Opt. Soc. Am. A* **20**, 40 (2003).
- [42] S. Marchesini, Invited article: A unified evaluation of iterative projection algorithms for phase retrieval, *Rev. Sci. Instrum.* **78**, 011301 (2007).
- [43] J. H. Seldin and J. R. Fienup, Numerical investigation of the uniqueness of phase retrieval, *J. Opt. Soc. Am. A* **7**, 412 (1990).
- [44] L.-H. Yeh, J. Dong, J. Zhong, L. Tian, M. Chen, G. Tang, M. Soltanolkotabi, and L. Waller, Experimental robustness of fourier ptychography phase retrieval algorithms, *Opt. Express* **23**, 33214 (2015).
- [45] M. Beckers, T. Senkbeil, T. Gorniak, M. Reese, K. Giewekemeyer, S.-C. Gleber, T. Salditt, and A. Rosenhahn, Chemical Contrast in Soft X-Ray Ptychography, *Phys. Rev. Lett.* **107**, 208101 (2011).
- [46] A. M. Maiden, G. R. Morrison, B. Kaulich, A. Gianoncelli, and J. M. Rodenburg, Soft x-ray spectromicroscopy using ptychography with randomly phased illumination, *Nat. Commun.* **4**, 1669 (2013).
- [47] R. M. Karl, Jr., G. Mancini, J. Knobloch, T. Frazer, J. Hernandez-Charpak, B. Abad, D. Gardner, E. Shanblatt, M. Tanksalvala, C. Porter, C. Bevis, D. Adams, H. Kapteyn, and M. Murnane, Full-field imaging of thermal and acoustic dynamics

- in an individual nanostructure using tabletop high harmonic beams, *Sci. Adv.* **4**, eaau4295 (2018).
- [48] W. Eschen, S. Wang, C. Liu, R. Klas, M. Steinert, S. Yulin, H. Meißner, M. Bussmann, T. Pertsch, J. Limpert, and J. Rothhardt, Towards attosecond imaging at the nanoscale using broadband holography-assisted coherent imaging in the extreme ultraviolet, *Commun. Phys.* **4**, 154 (2021).
- [49] S. Zayko, O. Kfir, M. Heigl, M. Lohmann, M. Sivilis, M. Albrecht, and C. Ropers, Ultrafast high-harmonic nanoscopy of magnetization dynamics, *Nat. Commun.* **12**, 6337 (2021).